ARTICLE

Relative Molecular Orientations in Organic Optoelectronic Films Probed via Polarization-Selected UV/IR Mixed Frequency Ultrafast Spectroscopy†

Chengzhen Shen, Jie Peng, Jianxin Guan, Chuangqing Hao, Zhihao Yu, Hong Jiang*, Junrong Zheng*

College of Chemistry and Molecular Engineering, Beijing National Laboratory for Molecular Sciences, Peking University, Beijing 100871, China

(Dated: Received on November 30, 2021; Accepted on December 25, 2021)

Molecular packing patterns are crucial factors determining electron/energy transfer processes that are critical for the optoelectronic properties of organic thin film devices. Herein, the polarization-selective ultraviolet/infrared (UV/IR) mixed frequency ultrafast spectroscopy is applied to investigate the relative molecular orientations in two organic thin films of 7-(diethylamino)coumarin-3-carboxylic acid (DEAC) and perylene. The signal anisotropy changes caused by intermolecular energy/electron transfers are utilized to calculate the cross angles between the electronic transition dipole moment of the donor and the vibrational transition dipole moments of the acceptor, yielding the relative orientation between two adjacent molecules. Using this method, the relative orientation angle in DEAC film is determined to be 53.4°, close to 60° of its single crystalline structure, and that of the perylene film is determined to be 6.2°, also close to −0.2° of its single crystalline structure. Besides experimental uncertainties, the small difference between the angles determined by this method and those of single crystals also results from the fact that the thin film samples are polycrystalline where some of the molecules are amorphous.

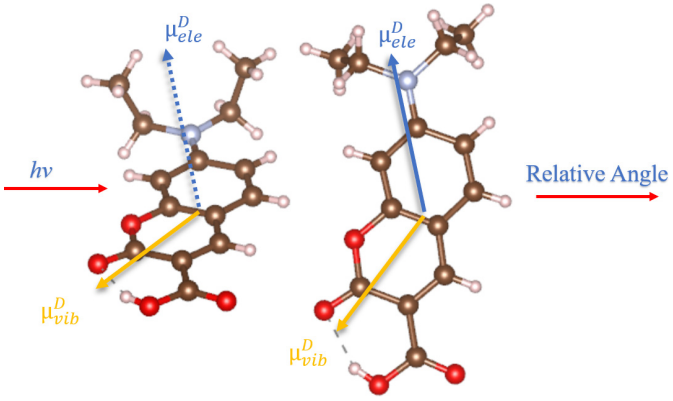

Key words: Optoelectronics, Relative molecular orientations, Organic films

I. INTRODUCTION

Organic materials are widely used in semiconductor devices, such as in organic field effect transistors (OFETs), light-emitting diodes (OLEDs), and photovoltaic cells (OPVs), due to their desirable properties, *e.g.* good flexibility, modifiability, and low-cost [1–4]. In these devices, the morphology and molecular packing patterns of the organic thin films have great impacts on their performance, especially the details of their microstructures because the local packing of neighboring molecules determines the intermolecular electronic orbital overlap and thus the electron/energy transfer dynamics. Routine techniques for organic material characterization include grazing-incidence X-ray diffraction (GIXD), atomic force microscopy (AFM), near-edge X-ray absorption fine structure (NEXAFS) spectroscopy and *etc.* [5–8]. They are extremely powerful. However, the morphology of organic materials is generally more complex than inorganic ones as the crystalline and

†Part of Special Issue "In Memory of Prof. Nanquan Lou on the occasion of his 100th anniversary".

*Authors to whom correspondence should be addressed. E-mail: jianghchem@pku.edu.cn, junrong@pku.edu.cn

amorphous domains often appear simultaneous in one organic film. Their molecular arrangements are also affected by the fragments or side chains of molecules. Because of the complexity, almost no single technique is able to completely resolve the packing arrangement of molecules inside a practical organic thin film but only by combining different techniques [5]. For example, GIXD gives the information of crystallographic structure, whereas AFM measures the surface morphology. Therefore, the development of new methods is essential to better characterize the microstructure of materials and thus understand the relationship between structure and properties, in particular, when current methods suffer from insufficient accuracy or resolution [6].

Ultrafast vibrational spectroscopy has been successfully applied to investigate molecular structures and ultrafast dynamics both in solids and in liquids, and is expected to gain wider applications for determining microstructures in molecular systems [9–19]. For example, the cross-angles of vibrational transition moment directions detected with two polarized ultrafast infrared pulses were used to determine the molecular conformations of 4′-methyl-2′-nitroacetanilide in different solutions and solid-states [16]. Besides, the relative intermolecular orientations in three polystyrene samples were probed based on the molecular heat transport via ultrafast two-dimensional infrared (2D-IR) and IR transient absorption methods [15]. In principle, both energy/heat transfer and vibrational cross angle methods are suitable for determining both inter- and intramolecular structures. Nevertheless, the signals in the methods to determine relative intermolecular orientations heavily rely on the initial vibrational excitation intensity and its relaxation channels, which require extremely high excitation power like narrowband picosecond lasers and are typically too weak to be detected with routine broadband femtosecond vibrational techniques. In this work, instead of using infrared exciting vibrations, ultraviolet is applied to excite electronic transitions, following which many intermolecular dynamic processes can occur, *e.g.* electron transfer, electronic energy transfer, vibrational energy transfer, and heat transfer. These dynamics can alter the vibrational transition frequencies and/or intensities of adjacent molecules, which can produce sufficiently strong signals for the detection of relative intermolecular orientations.

Two samples, 7-(diethylamino)coumarin-3-carboxylic acid (DEAC) and perylene, tested herein are polycyclic aromatic hydrocarbons with π-conjugated systems which have attracted an increasing amount of attention in recent years for various organic electronic devices. For instance, perylene [20, 21], as well as its derivatives, is used as non-fullerene acceptors for OPVs. DEAC is also widely used in fluorescence sensoring [22].

II. EXPERIMENTS AND MATERIALS

A. Ultrafast experiments and data analysis

Vibrational signals caused by intermolecular electron/energy transfers after electronic excitation are measured in real time using the polarization-selective ultraviolet/infrared (UV/IR) mixed frequency ultrafast spectroscopy. Briefly, UV/IR spectroscopy studies are performed with laser pulses (1 kHz, ∼50 fs pulse width, 800 nm central wavelength) from an amplified Ti/sapphire laser system (Uptek Solutions Inc.) which are split into two parts. One is used to pump a femtosecond OPA (TOPAS-Prime) producing ∼60 fs UV/visible pulses with a bandwidth ∼10 nm in a tunable wavelength range from 250 nm to 800 nm with ∼2 mW at 1 kHz. The other is used to pump another femtosecond OPA (Palitra, QUANTRONIX) producing mid-IR pulses with a bandwidth ∼200 cm^{-1} in a tunable frequency ranging from 1000 cm^{-1} to 3500 cm^{-1} with energy of ∼1 mW at 1 kHz. The UV/visible pulse excites the electron transition of the molecules and the excitation power is ∼200 μW with a spot diameter of 245 μm. The mid-IR pulse is used as the probe beam and collected by 2×64 pixel mercury cadmium telluride (MCT) detector (Infrared Associates). Two polarizers are inserted into the mid-IR beam pathway, one is located behind the sample to selectively measure the parallel or vertical polarized signal relative to the pump beam and another is before the sample, which is used to rotate the polarization of the probe beam about 45° relative to that of the pump beam. Polarization-selective signals are obtained by adjusting the relative polarizations of the two polarizers. Measuring the transmission of the mid-IR beam through the sample by chopping the pump beam at 500 Hz, the pump-probe signal $P(t)$ is collected and the lifetime is obtained from the rotation-free signal,

$$P(t) = \frac{P_{\parallel}(t) + 2P_{\perp}(t)}{3} \tag{1}$$

DOI:10.1063/1674-0068/cjcp2111260

and the anisotropy is calculated from the following equation:

$$r(t) = \frac{P_{\parallel}(t) - P_{\perp}(t)}{P_{\parallel}(t) + 2P_{\perp}(t)} \tag{2}$$

where $P_{\parallel}(t)$ and $P_{\perp}(t)$ are parallel and vertical signal (relative polarization between the pump and probe pulses), respectively. The anisotropy of a specific spectral signal or band can also be predicted from the cross angle (θ) between the absorption and emission dipole moments [23]:

$$r(t) = \frac{3\overline{\cos^2\theta} - 1}{5} \tag{3}$$

Two reasons may cause the anisotropic changes: the molecular rotation and the energy/heat/charge transfer among molecules [12]. Since the samples in this work are thin films and they are not plastic crystals, the molecular rotation can be ignored. If transfer happens from the excited molecule (donor) to an adjacent molecule (acceptor) which has a different orientation, the anisotropy will alter because of the change of the cross angle. For DEAC and perylene, the cross angle (θ) is that between the electronic and vibrational transition dipole moments. In this model, the initial anisotropy is determined by the cross angle (θ) between electronic transition ($\mu^{\mathrm{D}}_{\mathrm{ele}}$) and vibrational transition dipole moments ($\mu^{\mathrm{D}}_{\mathrm{vib}}$) in the donor molecule but after the transfer process a portion of the final anisotropy is attributed to the cross angle (θ) between electronic transition dipole moment of donor ($\mu^{\mathrm{D}}_{\mathrm{ele}}$) and vibrational transition dipole moment of the acceptor ($\mu^{\mathrm{A}}_{\mathrm{vib}}$), the cross angle change is shown in Scheme 1. Therefore, in turn we can calculate the two cross angles by the measured anisotropy in experiments, and then infer the relative orientation between molecules in the organic film. In addition, through exponentially fitting the anisotropic decays, we can obtain the transfer rate.

The samples are solution-casted on CaF_2 windows. The thicknesses of the samples are controlled to allow the vibrational absorptions of interest to have absorbance of about 0.5. The data analysis is not dependent on the sample thickness, but it is essential to have the right sample thickness to make sure there is enough IR light to be absorbed and to be detected. The method requires that within the laser focus spot the sample distribution must be random. Therefore, all the samples are prepared as polycrystalline and the size of each small crystalline domain is much smaller than the laser focus spot which is about 100−200 microns.

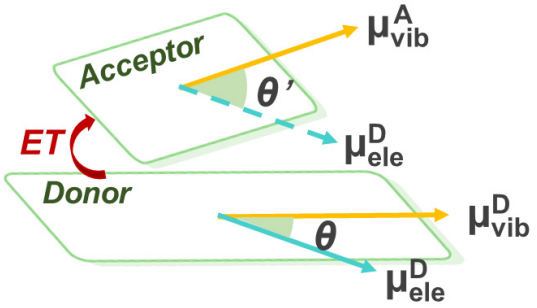

Scheme 1. Illustrated change of the cross angle before transfer (θ) and after transfer (θ'). $\mu^{\mathrm{D}}_{\mathrm{vib}}$ and $\mu^{\mathrm{A}}_{\mathrm{vib}}$ are the vibrational transition dipole moments of the donor and the acceptor, $\mu^{\mathrm{D}}_{\mathrm{ele}}$ is the electronic transition dipole moment of the donor.

B. Computational methods

The geometries and vibrational frequencies of 9,9′BF, perylene and DBC are optimized and computed with the B3LYP [24] method and 6-31++G(d,p) basis set. All the calculations are performed with Gaussian 09 software [25]. Scaling factor of 0.9648 was used to improve description of spectra [26].

III. RESULTS AND DISCUSSION

The molecular structures of DEAC and perylene and their normalized UV-visible and IR absorption spectra are displayed in FIG. 1. DEAC has two distinct absorption bands in the UV-visible spectrum, where the band at the short wavelength (below 350 nm) is attributed to the π-π^* transitions of the fluorene units and the band at 450 nm corresponds to the transition of the full conjugated structure. The absorption spectrum of perylene has three peaks respectively at 388, 409, and 437 nm which show vibronic features of the electronic transition from S_0 to S_1. FIG. 1(c) shows the FTIR absorption spectra of DEAC between 1400 cm^{-1} and 1650 cm^{-1} and perylene between 1300 cm^{-1} and 1550 cm^{-1}. For DEAC, three absorption peaks at 1510 cm^{-1}, 1575 cm^{-1} and 1606 cm^{-1} which belong to the vibrations of aromatic rings are chosen for time-resolved study. Perylene has three vibrational absorption bands at 1332 cm^{-1}, 1380 cm^{-1}, and 1500 cm^{-1}, which are

DOI:10.1063/1674-0068/cjcp2111260

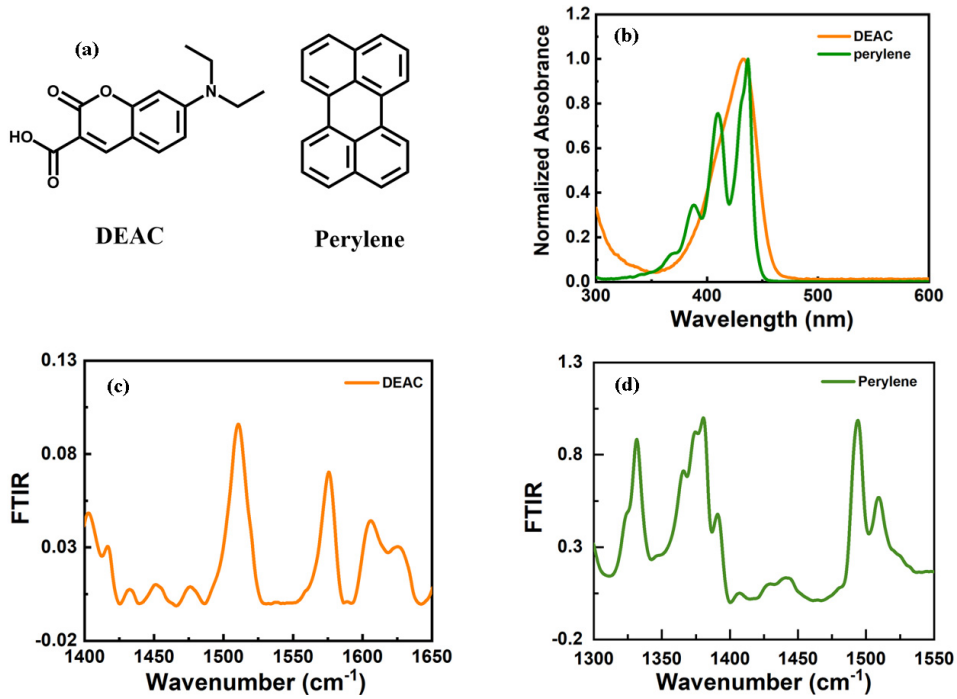

FIG. 1 (a) Chemical structures of DEAC and perylene. (b) Normalized UV-Vis absorption spectra of DEAC in 2.9×10^{-6} mol/L CH_2Cl_2 and perylene in 1×10^{-5} mol/L THF. (c) Normalized FTIR absorption spectra of DEAC and perylene films.

also attributed to the vibrations of aromatic rings.

FIG. 2 displays the ultrafast UV/IR spectra at different delay time and the anisotropy decays of DEAC and perylene films after excitation with photons of 400 nm. The reason to choose 400 nm rather than the absorption peak central wavelength ∼437 nm is to relieve the transition dipole moment mismatch between the electronic (big) and vibrational (small) excitations. For the film of DEAC three absorption peaks at 1515, 1584, and 1614 cm^{-1} in FIG. 2(a) appear upon UV excitation. The peaks reach maxima almost instantaneously within the temporal resolution of the excitation and decrease rapidly. These peaks slightly blueshift, compared to the peaks located at 1510, 1575, and 1606 cm^{-1} in the FTIR spectra in FIG. 1(c), caused by the excited state absorption of the vibrational modes of the aromatic rings and frequency shifts induced by the electronic excitation. Similarly, FIG. 2(c) shows the UV/IR spectra of perylene film between 1300 and 1550 cm^{-1} excited by 400 nm. As can be seen from the figure, there are several obvious excited state absorption peaks in agreement with the FTIR spectra which are assigned to different vibration modes of the benzene skeleton. FIG. 2(b, d) show the intensities and exponential fitting curves of main vibration modes of the two molecules, and the results of time constants will be discussed below.

FIG. 3(a) displays the anisotropies of absorption peaks of DEAC. The values and the decay tendencies of the anisotropy at 1515 cm^{-1} and 1584 cm^{-1} are almost the same and decay exponentially from 0.172 to −0.012 within 150 ps. As mentioned above, the anisotropic decay here is attributed to the energy/electron/heat transfer processes between adjacent molecules with different orientations. Contrast to DEAC of which the anisotropies at different wavelengths have the same dynamics, different vibration modes of perylene exhibit two different dynamics. The anisotropies at 1332 cm^{-1} and 1380 cm^{-1} remain within 30 ps, whereas those of 1493 cm^{-1} and 1510 cm^{-1} show similar exponential growth from 0 to 0.032 and from 0.038 to 0.072, respectively (FIG. 3(c) and FIG. S1 in Supplementary matrials (SM) which illustrates that fast transfer processes occur among adjacent molecules. Peaks at 1380 cm^{-1} and 1493 cm^{-1} will be discussed in the following. Given that the anisotropy change is directly related to the direction of the vibrational transition dipole moments of the donor and the acceptor molecules, we speculate that the vibrational transition dipole moments of 1515 cm^{-1} and 1584 cm^{-1} for DEAC are the same, while that of 1380 cm^{-1} and 1493 cm^{-1} for perylene are different,

DOI:10.1063/1674-0068/cjcp2111260

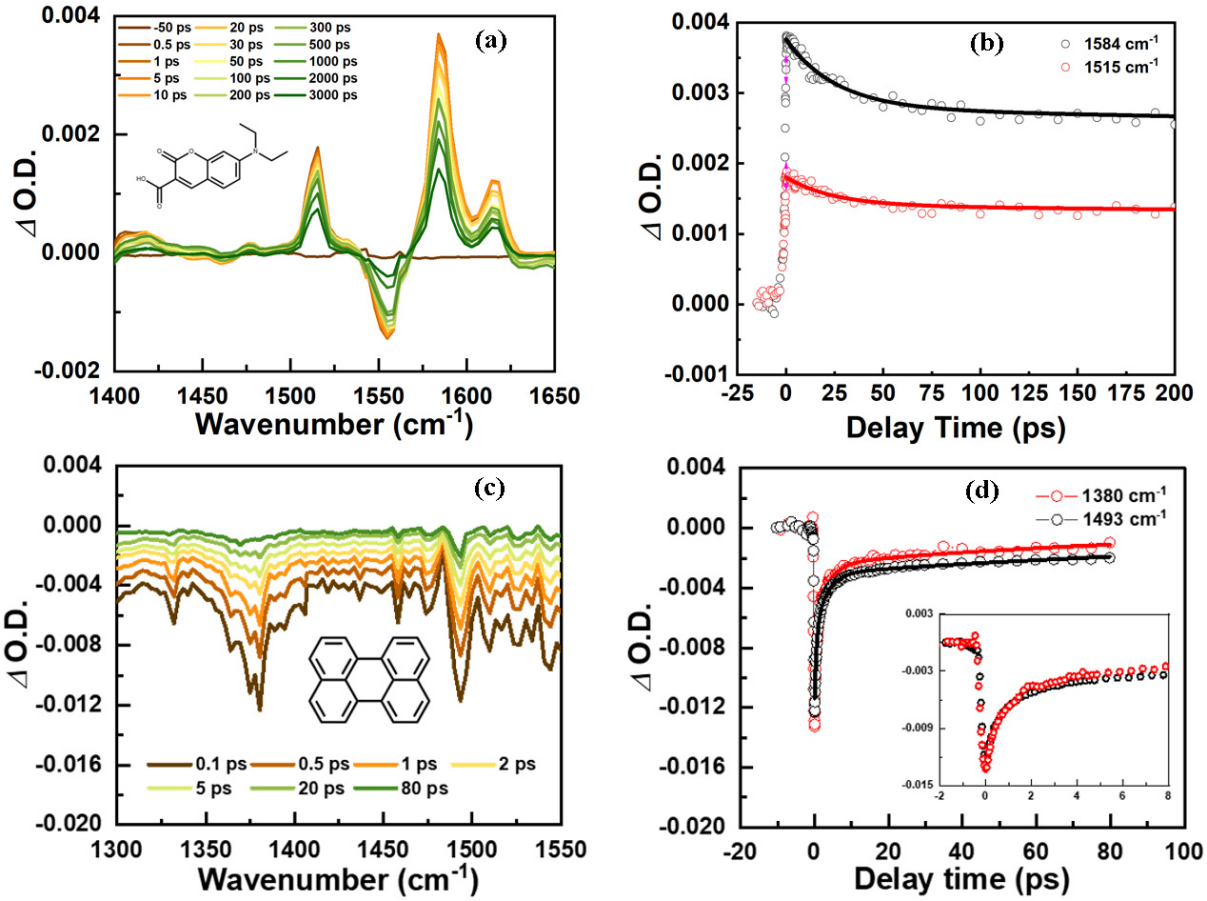

FIG. 2 The UV/IR mixed frequency ultrafast spectra at different delay time of (a) the DEAC excited at 400 nm and (c) the perylene film excited at 400 nm. Peak intensities of (b) DEAC at 1515 cm^{-1} and 1584 cm^{-1} and (d) perylene at 1380 cm^{-1} and 1493 cm^{-1} with their exponential fitting curves after 100 fs.

which is supported by the calculated results [27].

Decay dynamics of each vibrational modes and corresponding anisotropy information of DEAC and perylene are shown in Table I, FIG. 2, and FIG. S1 in SM. As discussed above, the alteration of the anisotropy is caused by electron/energy transfers from the excited molecule to a neighbouring molecule. In perylene, the anisotropies of 1493 cm^{-1} and 1510 cm^{-1} have a similar decay time constant, ∼2.7 ps, which is also approximately the energy/electron transfer rate. The vibrational dynamics of perylene can be best fitted by a three-exponential function. Firstly, an ultrafast relaxation process within 0.5 ps is probably because of the decay of the free electron due to the photoexcitation [28–30]. Secondly, the decay time ∼3.3 ps for perylene is probably because of the vibrational relaxation of the mode. Last, the longest lifetime of them (over 100 ps) reflects the decay of the excited electronic state [31] and heat dissipation. The vibrational dynamics of DEAC can be best fitted by a two-exponential function. The faster one is related to the vibrational relaxation process of the breathing modes of the aromatic rings while the slower one might give information about the electronic decay.

We propose a mathematical model to analyze the anisotropy decay dynamics. The transfer process from the donor to the acceptor as well as the rotation of the molecules can cause the anisotropy decay [32], and it can also go back from the acceptor with a certain probability which recovers the anisotropy value. Therefore, at each time t, $r(t)$ corresponds to the sum of the anisotropies of donor and acceptor molecules. After a period of time, transfers reach balance and the anisotropy decays to a constant eventually. The sample films are polycrystalline, and the orientation of the excited molecules is random. To simplify the problem, we assume that the film can be divided into many tiny crystals and the transfer process only happens within

DOI:10.1063/1674-0068/cjcp2111260

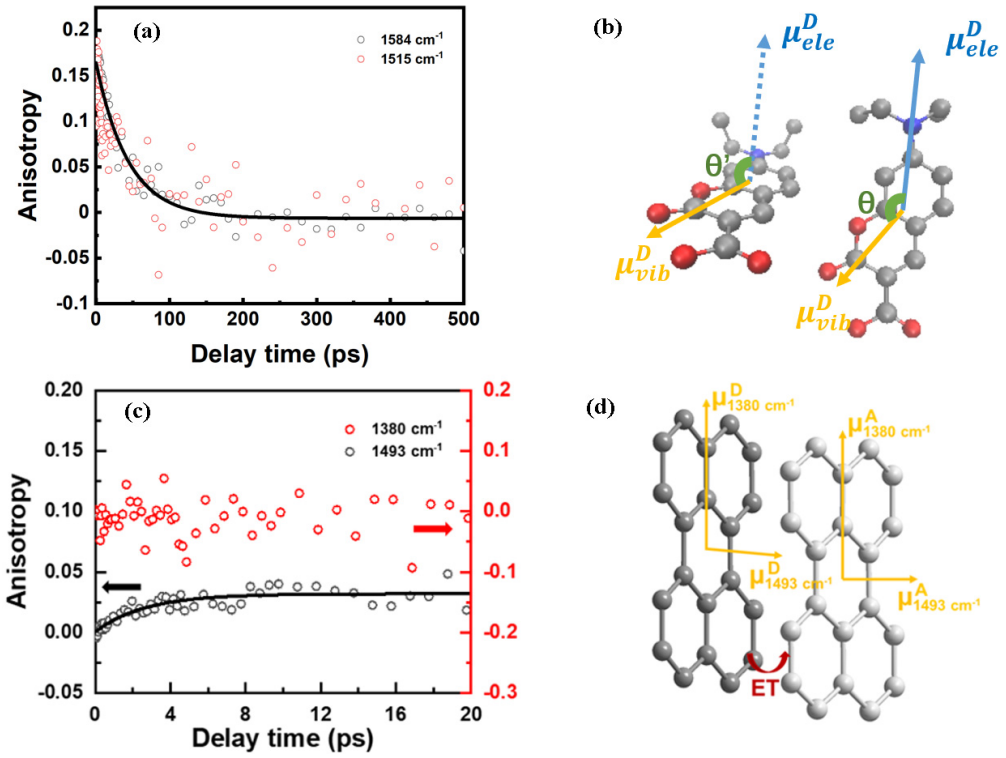

FIG. 3 Anisotropies of the main peaks of (a) DEAC at 1515 cm^{-1} and 1584 cm^{-1}, (c) perylene at 1380 cm^{-1} and 1493 cm^{-1}. Illustrated molecular orientations and processes of intermolecular energy transfer in the film of (b) DEAC and (d) perylene. The directions of electronic and vibrational transition dipole moments are denoted by blue and yellow arrows, respectively, and θ and θ' denote the cross angles between the electronic transition dipole moment of donor and the vibrational transition dipole moments of donor and accepters.

TABLE I Exponential fitting results for the main peaks and their anisotropies of DEAC and perylene film.

Compound	Wavenumber/cm^{-1}	τ_1/ps	τ_2/ps	τ_3/ps	Anistropy/ps
DEAC	1515	24.35±2.92	5120.93±268.93		36.65±5.80
	1584	25.88±1.90	5164.16±203.26		43.82±2.89
	1614	29.01±2.54	6085.95±582.54		51.86±6.80
Perylene	1332	0.28±0.02	2.41±0.08	104.46±11.55	
	1380	0.52±0.01	3.41±0.09	103.22±6.58	
	1493	0.46±0.01	3.17±0.04	172.38±5.48	2.65±0.30
	1510	0.44±0.01	3.52±0.05	145.53±6.67	2.69±0.75

each crystal. We also assume that the molecules have only two orientations in the crystal initially. The total concentration of excited molecules is denoted as y. At time t, the concentration of excited molecules which have the same/different orientations as just excited is denoted as y_1/y_2. We can easily find:

$$y = y_1 + y_2 \tag{4}$$

In our systems, transfer occurs between same species which means it will not change y, while it can change y_1 and y_2. Thus we can assume the decay of y fulfills the single-exponential function:

$$y = C_0 e^{-k_1 t} \tag{5}$$

C_0 is the initial concentration and k_1 is the decay rate constant. We can also obtain differential Eq.(6) and Eq.(7):

$$\frac{dy_1}{dt} = \frac{1}{n+1}ky_2 - \frac{n}{n+1}ky_1 - k_1 y_1 \tag{6}$$

$$\frac{dy_2}{dt} = \frac{n}{n+1}ky_1 - \frac{1}{n+1}ky_2 - k_1 y_2 \tag{7}$$

DOI:10.1063/1674-0068/cjcp2111260

where k is the transfer rate constant, and n represents the ratio of acceptor to donor in the crystal. Combining Eq.(4) with Eq.(6), we can obtain a differential equation (Eq.(8)) about y_1:

$$\frac{\mathrm{d}y_1}{\mathrm{d}t} = \frac{1}{n+1}kC_0\mathrm{e}^{-k_1t} - (k+k_1)\,y_1 \tag{8}$$

To solve Eq.(8), we introduce m which satisfies:

$$m = \mathrm{e}^{-k_1t} \tag{9}$$

$$\mathrm{d}m = -k_1m\mathrm{d}t \tag{10}$$

We can get a linear differential equation:

$$\frac{\mathrm{d}y_1}{\mathrm{d}m} - \frac{k+k_1}{k_1m}y_1 = -\frac{kC_0}{(n+1)\,k_1} \tag{11}$$

Solving Eq.(11):

$$y_1 = \frac{C_0}{n+1}m + Cm^{(k+k_1)/k_1} \tag{12}$$

At t=0, y_1 is equal to y, so we can get:

$$y_1 = \frac{C_0}{n+1}\mathrm{e}^{-k_1t} + \frac{nC_0}{n+1}\mathrm{e}^{-(k+k_1)t} \tag{13}$$

Also, we can get y_2:

$$y_2 = \frac{nC_0}{n+1}\mathrm{e}^{-k_1t} - \frac{nC_0}{n+1}\mathrm{e}^{-(k+k_1)t} \tag{14}$$

Assuming the angle of y_1 as θ, the angle of y_2 as θ':

$$\begin{aligned}\overline{\cos^2\theta} &= \frac{\cos^2\theta y_1 + \cos^2\theta' y_2}{y} \\ &= \frac{1}{n+1}\left(\cos^2\theta + n\cos^2\theta'\right) \\ &\quad + \frac{n}{n+1}\mathrm{e}^{-kt}\left(\cos^2\theta - \cos^2\theta'\right)\end{aligned} \tag{15}$$

Substituting Eq.(15) into Eq.(3), we can get the relationship between $r(t)$ and t:

$$\begin{aligned}r\,(t) = \frac{3}{5}\Bigg[&\frac{1}{n+1}\left(\cos^2\theta + n\cos^2\theta'\right) \\ &+ \frac{n}{n+1}\mathrm{e}^{-kt}\left(\cos^2\theta - \cos^2\theta'\right)\Bigg] - \frac{1}{5}\end{aligned} \tag{16}$$

From Eq.(16), we can get

$$r(0) = \frac{3\cos^2\theta - 1}{5}$$

$$r\,(\infty) = \frac{3\left(\cos^2\theta + n\cos^2\theta'\right) - (n+1)}{5\,(n+1)}$$

here $r(0)$ only reflects the angle at the same molecule, $r\,(\infty)$ means the transfer process reaches the final balance. The equation decay rate constant of $r(t)$ is k, which is also the transfer rate constant.

According to the crystal structure of DEAC [33], there are only two orientations, so that n=1. Therefore,

$$\begin{aligned}r(t) = \frac{3}{5}\Bigg[&\frac{1}{2}\left(\cos^2\theta + \cos^2\theta'\right) \\ &+ \frac{1}{2}\mathrm{e}^{-kt}\left(\cos^2\theta - \cos^2\theta'\right)\Bigg] - \frac{1}{5}\end{aligned} \tag{17}$$

From the measured results of DEAC exhibited in FIG. 3, $r(0)$=0.172, $r(\infty)$=−0.012. According to Eq.(17) we can get the cross angle between the electronic transition of the excited donor molecule and the vibrational dipole moment of the donor/acceptor, θ=37.65° and θ'≈90°. Here, we assume that the molecules is planar. The relative angle between two molecules is thus derived to be approximately 53.35° in the thin film, which is close to that in the crystalline structure, 60° determined by XRD.

With the same method, we can get the same equation as Eq.(17) for perylene according to the crystal structure and the measured data in FIG. 3 and Table I.

The ratio of acceptor with different orientation and molecules with the same orientation is 1, so n=1. For 1493 cm^{-1}, $r(0)$=0, $r(\infty)$=0.032. From Eq.(17) and the initial and final anisotropies, we can calculate the cross angles between transition dipole moments, that is θ=54.7° and θ'=48.5° and the relative angle between two adjacent molecules is 6.2°. The calculated vibrational transition dipole moments of 1380 cm^{-1} and 1493 cm^{-1} have different directions [27], which are parallel and perpendicular to the long axis of perylene, respectively. The calculated electronic transition dipole moment is along the long axis of perylene too. The anisotropy of 1493 cm^{-1} changes due to the difference between anisotropies of the donor and the acceptor, while the anisotropy of 1380 cm^{-1} remains constant because θ and θ' at 1380 cm^{-1} are the same. In other words, vibrational transition dipole moments of the donor and the acceptor at 1380 cm^{-1} have the same direction. Therefore, we can deduce that the donor and the acceptor are parallel to each other in the long axis

DOI:10.1063/1674-0068/cjcp2111260

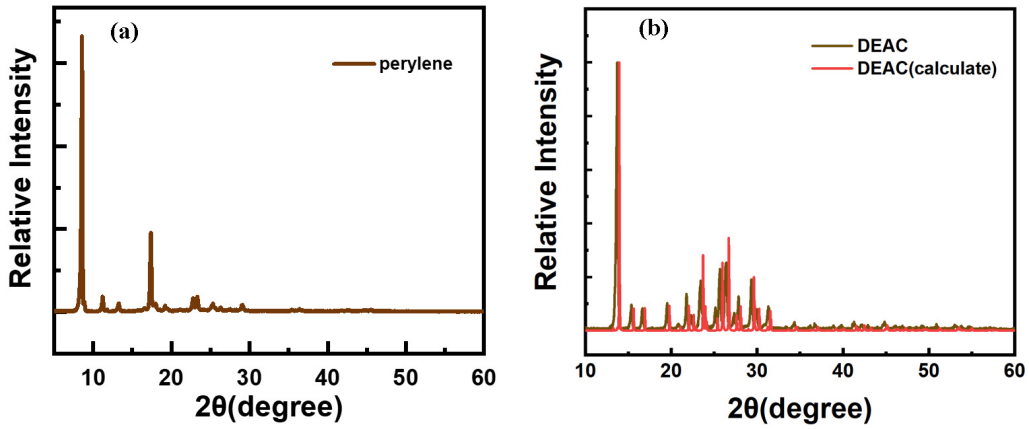

FIG. 4 XRD data of (a) perylene film and (b) DEAC film.

direction, but have a dihedral angle, 6.2°, in the short axis direction. The values are close to −0.2° determined by XRD.

Practically, in organic films, many molecules are at the "amorphous" state, which can be seen from XRD data in FIG. 4 in which the peaks are broader than those of single crystals. These "amorphous" molecules can be ordered within the range of a few molecules but disordered in larger ranges, and cause the molecular cross angle measured by the method slightly different from those of the crystals, because the relative molecular orientation measurements provide the average molecular local packing information within the laser focus spot rather than only the crystalline domains. Combined with the crystalline structure, the relative orientation results can give us additional information about the packing pattern in the "amorphous" state. For example, based on the value 6.2° from the orientation measurements, and −0.2° from XRD, the molecules inside the amorphous state of the perylene sample are estimated to be stacked with a dihedral angle bigger than 20° in the short axis direction (assuming <10% amorphous state), which is obviously larger than that in the crystalline domains. The detailed value of this angle requires information about the crystallinity and the relative contribution to the experimental signal by the molecules in the two states, which will be subject to future studies.

IV. CONCLUSION

In this work, the polarization-selective UV/IR mixed frequency ultrafast spectroscopy is used to probe the relative molecular orientations in the thin films of DEAC and perylene. The relative angle between adjacent DEAC molecules is determined to be 53.35°, and two adjacent perylenes are parallel to each other in the long axis direction, but have a small angle of 6.2° in the short axis direction. The results are close to those determined by XRD, demonstrating the feasibility of the method. However, the mathematical model to analyze data contains several assumptions like a planar molecular structure that can cause uncertainty. The two samples studied in this work are mostly crystalline. In principle, this method and its mathematical model can be further developed and generalized to determine the relative orientation of molecules which are locally ordered within the size of a few nanometers or smaller but amorphous in larger dimensions in films.

Supplementary materials: Molecular source, supporting spectral results are available. Anisotropies and intensities of perylene (FIG. S1) and DEAC (FIG. S2) are given.

V. ACKNOWLEDGEMENTS

This work is supported by Ministry of Science and Technology of China (No.2017YFA0204702) and the National Natural Science Foundation of China (No.21627805, No.21673004, No.21804004, and No.21821004).

[1] H. Sirringhaus, Adv. Mater. **26**, 1319 (2014).
[2] Y. Z, Lin, Y. F. Li, and X. W. Zhan, Chem. Soc. Rev. **41**, 4245 (2012).
[3] C. L. Wang, H. L. Dong, L. Jiang, and W. P. Hu, Chem. Soc. Rev. **47**, 422 (2018).

DOI:10.1063/1674-0068/cjcp2111260

[4] A. Facchetti, Chem. Mater. **23**, 733 (2011).
[5] D. M. Delongchamp, R. J. Kline, D. A. Fischer, L. J. Richter, and M. F. Toney, Adv. Mater. **23**, 319 (2011).
[6] J. Rivnay, S. C. B. Mannsfeld, C. E. Miller, A. Salleo, and M. F. Toney, Chem. Rev. **112**, 5488 (2012).
[7] Y. Xiao and X. Lu, Mater. Today Nano **5**, 100030 (2019).
[8] A. Salleo, R. J. Kline, D. M. DeLongchamp, and M. L. Chabinyc, Adv. Mater. **22**, 3812 (2010).
[9] H. T. Bian, H. L. Chen, J. B. Li, X. W. Wen, and J. R. Zheng, J. Phys. Chem. A **115**, 11657 (2011).
[10] H. L. Chen, H. T. Bian, J. B. Li, X. M. Guo, X. W. Wen, and J. R. Zheng, J. Phys. Chem. B **117**, 15614 (2013).
[11] Y. N. Shen, T. M. Wu, B. Jiang, G. H. Deng, J. B. Li, H. L. Chen, X. M. Guo, C. Q. Ge, Y. J. Chen, J. Y. Hong, X. M. Yang, Y. J. Yuan, W. Zhuang, and J. R. Zheng, J. Phys. Chem. B **119**, 9893 (2015).
[12] H. T. Bian, X. W. Wen, J. B. Li, and H. L. Chen, Proc. Natl. Acad. Sci. USA **108**, 4737 (2011).
[13] H. T. Bian, J. B. Li, X. W. Wen, Z. G. Sun, J. Song, W. Zhuang, and J. R. Zheng, J. Phys. Chem. A **115**, 3357 (2011).
[14] F. Liu, W. J. Wu, Y. S. Bai, S. H. Chae, Q. Y. Li, J. Wang, J. Hones, and X. Y. Zhu, Science **367**, 903 (2020).
[15] G. D. Scholes, G. R. Fleming, L. X. Chen, A. Aspuru-Guzik, A. Buchleitner, D. F. Coker, G. S. Engel, R. Grondelle, A. Ishizaki, D. M. Jonas, J. S. Lundeen, J. K. McCusker, S, Mukamel, J. P. Ogilvie, A. O. Castro, M. A. Ratner, F. C. Spano, K. B. Whaley, and X. Y. Zhu, Nature **543**, 647 (2017).
[16] H. L. Chen, Y. F. Zhu, J. B. Li, H. J. Liu, D. E. Jiang, and J. R. Zheng, J. Phys. Chem. A **117**, 840 (2013).
[17] C. Grieco, G. S. Doucette, J. M. Munro, E. R. Kennehan, Y. Lee, A. Rimshaw, M. M. Payne, N. Wonderling, J. E. Anthony, I. Dabo, E. D. Gomez, and J. B. Asbury, Adv. Funct. Mater. **27**, 1703929 (2017).
[18] H. L. Chen, X. W. Wen, J. B. Li, and J. R. Zheng, J. Phys. Chem. A **118**, 2463 (2014).
[19] C. Grieco, E. R. Kennehan, H. Kim, R. D. Pensack, Al. N. Brigeman, A. Rimshaw, M. M. Payne, J. E. Anthony, N. C. Giebink, G. D. Scholes, and J. B. Asbury, J. Phys. Chem. C **122**, 2012 (2018).
[20] A. G. Macedo, L. P. Christopholi, A. E. X. Gavim, J. F. de Deus, M. A. M. Teridi, A. R. M. Yusoff, and W. J. Silva, J. Mater. Sci. Mater. Electron. **30**, 15803 (2019).
[21] S. Wirsing, M. Hansel, V. Belova, F. Schreiber, K. Broch, B. Engels, and P. Tegeder, J. Phys. Chem. C **123**, 27561 (2019).
[22] Y. M. Ma, W. Luo, P. J. Quinn, and Z. D. Liu, J. Med. Chem. **47**, 6349 (2004).
[23] P. J. Stephens, F. J. Devlin, C. F. Chabalowski, and M. J. Frisch, J. Phys. Chem. **98**, 11623 (1994).
[24] M. J. Frisch, G. W. Trucks, H. B. Schlegel, G. E. Scuseria, M. A. Robb, J. R. Cheeseman, G. Scalmani, V. Barone, G. A. Petersson, H. Nakatsuji, X. Li, M. Caricato, A. V. Marenich, J. Bloino, B. G. Janesko, R. Gomperts, B. Mennucci, H. P. Hratchian, J. V. Ortiz, A. F. Izmaylov, J. L. Sonnenberg, D. Williams-Young, F. Ding, F. Lipparini, F. Egidi, J. Goings, B. Peng, A. Petrone, T. Henderson, D. Ranasinghe, V. G. Zakrzewski, J. Gao, N. Rega, G. Zheng, W. Liang, M. Hada, M. Ehara, K. Toyota, R. Fukuda, J. Hasegawa, M. Ishida, T. Nakajima, Y. Honda, O. Kitao, H. Nakai, T. Vreven, K. Throssell, J. A. Montgomery, Jr., J. E. Peralta, F. Ogliaro, M. J. Bearpark, J. J. Heyd, E. N. Brothers, K. N. Kudin, V. N. Staroverov, T. A. Keith, R. Kobayashi, J. Normand, K. Raghavachari, A. P. Rendell, J. C. Burant, S. S. Iyengar, J. Tomasi, M. Cossi, J. M. Millam, M. Klene, C. Adamo, R. Cammi, J. W. Ochterski, R. L. Martin, K. Morokuma, O. Farkas, J. B. Foresman, and D. J. Fox, *Gaussian 16, Revision A.03*, Wallingford, CT: Gaussian, Inc. (2016).
[25] J. P. Merrick, D. Moran, and L. Radom, J. Phys. Chem. A **111**, 11683 (2007).
[26] K. K. Ong, J. O. Jensen, and H. F. Hameka, J. Mol. Struct.: THEOCHEM **459**, 131 (1999).
[27] J. R. Lakowicz, *Principles of Fluorescence Spectroscopy*, Boston: Springer, 954 (2006).
[28] X. W. Wen, H. L. Chen, T. M. Wu, Z. H. Yu, Q. R. Yang, J. W. Deng, Z. T. Liu, X. Guo, J. X. Guan, X. Zhang, Y. J. Gong, J. T. Yuan, Z. H. Zhang, C. Y. Yi, X. F. Guo, P. M. Ajayan, W. Zhuang, Z. R. Liu, J. Lou, and J. R. Zheng, Nat. Commun. **9**, 1 (2018).
[29] W. J. Zhang, C. P. Chuu, J. K. Huang, C. H. Chen, M. L. Tsai, Y. H. Chang, C. T. Liang, Y. Z. Chen, Y. L. Chueh, J. H. He, M. Y. Chou, and L. J. Li, Sci. Rep. **4**, 1 (2015).
[30] L. M. Malard, K. F. Mak, A. H. C. Neto, N. M. R. Peres, and T. F. Heinz, New J. Phys. **15**, (2013).
[31] J. Conyard, I. A. Heisler, W. R. Browne, B. L. Feringa, S. Amirjalayer, W. J. Buma, S. Woutersen, and S. R. Meech, J. Phys. Chem. A **118**, 5961 (2014).
[32] K. J. Gaffney, I. R. Piletic, and M. D. Fayer, J. Chem. Phys. **118**, 2270 (2003).
[33] G. R. Bardajee, M. A. Winnik, and A. J. Lough, Acta Crystallogr. Sect. E: Struct. Rep. Online **62**, o3076 (2006).

DOI:10.1063/1674-0068/cjcp2111260